ISSN (Print) : 2337-9030 ISSN (Online) : 2685-2608
PILLAR OF PHYSICS
JURNAL BERKALA ILMIAH FISIKA
Vol. 19 (1), 2026, page. 01-08
DOI : https://doi.org/10.24036/axdg7y88

Analysis of the Effects of Proton Energy and Silicon Detector Thickness on the Total Ionizing Dose (Tid) Using Phits Monte Carlo Simulation

Sitti Yani[1*], Siti Karmilah Syahri Fartini[1], Rima Fitria Adiati[1], Tony Sumaryada[1]

[1] *Department of Physics, Faculty of Mathematics and Natural Sciences, IPB University, Jl. Meranti Kampus IPB Dramaga, Bogor 16680, Indonesia*
Corresponding author. Email: sittiyani@*apps.ipb.ac.id*

ABSTRACT

This study analyzes the effects of proton energy and silicon detector thickness on particle distribution and dosimetric response using Monte Carlo simulations based on the Particle and Heavy Ion Transport System (PHITS) code. Simulations were performed at two proton energies, namely 25 MeV and 100 MeV, with variations in silicon detector thickness grouped into thin and bulk categories. The analyzed results include the two-dimensional distributions of protons, secondary photons, and secondary neutrons, as well as the Total Ionizing Dose (TID) values in the silicon detector. The simulation results show that the proton distribution is clearly influenced by particle energy, where 100 MeV protons have a longer transport range and more dominant penetration compared to 25 MeV protons. Conversely, visual differences in the distribution of secondary particles, namely photons and neutrons, across all energy and thickness variations are not clearly apparent in the obtained two-dimensional maps. From a dosimetric perspective, TID increases linearly with increasing silicon detector thickness for both proton energies. Furthermore, the TID values at 100 MeV are consistently higher than those at 25 MeV across all thickness variations. Analysis of the $D_{100}(t)/D_{25}(t)$ ratio indicates that an increase in proton energy enhances the dosimetric response at every detector thickness. These results confirm that within the detector thickness range of 0.001 cm to 0.5 cm, thickness directly determines the magnitude of TID, while proton energy enhances the detector's dosimetric response.

Keywords : Silicon Detector; Total Ionizing Dose (TID); Monte Carlo; PHITS

I. INTRODUCTION

Total Ionizing Dose (TID) is a dosimetry parameter that represents the energy of ionizing radiation absorbed per unit mass of material; it is widely used to evaluate the effects of radiation on semiconductor materials, sensors, and electronic devices operating in radiation environments [1-3]. The quality and quantity of radiation are represented by the dose, which describes the magnitude of energy deposition that can potentially affect the performance of materials or devices, and by the particle flux passing through. The relevance of TID in silicon-based systems is also evident in various studies of devices and detectors, including studies of the TID effect on electronic devices and the use of silicon plates as the sensitive volume for TID evaluation in shielding configurations [4], [5].

Several factors influence the magnitude of TID in silicon detectors, including the type and energy of the incident particles and the thickness of the detector's sensitive volume [6], [7]. Proton energy determines penetration capability, interaction path length, and the probability of secondary particle formation, while detector thickness determines the size of the active volume that receives energy deposition. Previous research has shown that the thickness of the silicon detector is a critical parameter in radiation response, whether in thin detectors or thicker structures; for example, studies on ultra-thin silicon detectors report thicknesses ranging from a few to tens

of micrometers, while other studies highlight the importance of silicon thickness in evaluating radiation response and energy deposition [8].

Monte Carlo simulations have long been used to analyze dosimetric responses and particle transport in semiconductor materials because they can model radiation interactions in detail across a wide range of energy scales and geometries, including TID calculations [9-12]. Park et al. (2019) performed a Geant4-based Monte Carlo simulation to model an X-ray inspection system and calculate the absorbed dose in semiconductor components, demonstrating that this absorbed dose is highly dependent on X-ray energy [9]. Other studies have also specifically examined the ability of MCNPX Monte Carlo to track the transport of neutron particles within semiconductor detectors [11].

This study aims to analyze the effects of proton energy and silicon detector thickness on the Total Ionizing Dose using Monte Carlo simulations based on the Particle and Heavy Ion Transport code System (PHITS). Simulations were performed at two proton energies, namely 25 MeV and 100 MeV, with variations in silicon detector thickness grouped into two main categories: thin and bulk. In addition to evaluating TID values across all thickness variations, this study also analyzed the distribution of protons and secondary particles—namely photons and neutrons—to support the interpretation of the physical mechanisms underlying the dosimetric response.

II. METHOD

1) *Simulation Design*: All simulations in this study were performed using the Monte Carlo-based Particle and Heavy Ion Transport code System (PHITS) [13]. Simulations were performed to evaluate the effect of silicon detector thickness on the dose response following the production of secondary particles in an aluminum alloy (Al alloy) target with the following elemental composition: Mg, Al, Si, Ti, Cr, Mn, Fe, Cu, and Zn, with a weight fraction of 0.025000, 0.892500, 0.002340, 0.001170, 0.002300, 0.001760, 0.002930, 0.016000, and 0.056000, respectively. The simulation design was developed to calculate the differences in dose values resulting from variations in the thickness of the volume-sensitive region, with all silicon detectors placed at the same depth. The density of Al alloy and Si are 2.81 and 2.33 g/cm^3, respectively.

The simulation geometry is shown in Figure 1 below. The geometry was constructed in a linear configuration along the z-axis, a target material for secondary particle production, an air gap, and a silicon detector. The air gap between Al alloy and Si have density 0.001205 g/cm^3 that consist of O, N, C, and H with weight fraction 0.7874, 0.2123, 0.0001 and 0.0002, respectively. The protons are 1 cm directed toward an Al alloy target to generate a secondary particle field, which subsequently interacts with the silicon-sensitive volume. A linear geometry was chosen to simplify the interpretation of particle transport mechanisms and energy deposition while minimizing geometric complexity. The simulated proton energies are 25 and 100 MeV. These two energies were selected to represent two distinct shielding response regimes: the intermediate-energy condition, where protons can be completely stopped by the shielding material, and the high-energy condition, where most protons still possess significant penetration capability through a 5-mm-thick shield, allowing TID to be measured under conditions dominated by both stopping and penetration processes.

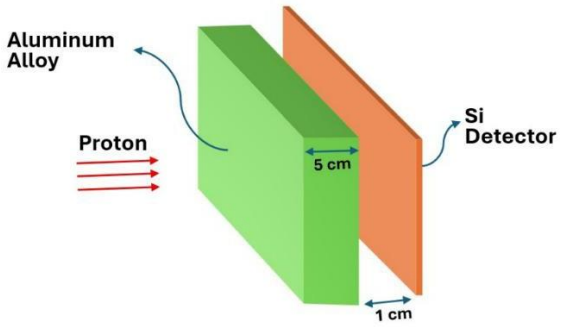

Fig. 1. Simulation design

The range of silicon thicknesses used in this study is from 0.001 cm to 0.5 cm. This range was chosen to cover two thickness regimes: thin and bulk. The thin group covers thicknesses of 0.001–0.02 cm, and the bulk group covers 0.1–0.5 cm. This grouping is intended to facilitate the analysis of changes in dosimetric response from a very shallow sensitive volume to a much larger active volume. Simulations were run under identical source, target, material, and geometric environment conditions for all thickness variations. The primary simulation output was obtained through the tally of energy deposition in the detector volume, while additional tallies could be used to support the interpretation of the distribution of secondary particle tracks within the simulation geometry.

2) *TID Calculation*: The primary parameter analyzed is the Total Ionizing Dose (TID), which is a quantity that represents the energy of ionizing radiation absorbed by a material per unit mass. In this simulation, TID is used to assess how changes in the thickness of the silicon sensitive volume affect the dose received by the detector when exposed to a secondary particle field resulting from the interaction of primary particles with the target. The TID value is obtained from the t-deposit in the silicon volume with the output in the form of a dose, so that each simulation result represents the amount of dose absorbed by the detector for the specified irradiation conditions.

Dose (D) is defined as the energy deposited (E_{dep}) in a material divided by the mass (m) of that material [14], [15], which can be expressed mathematically as the following equation (1).

$$D = \frac{E_{dep}}{m} \tag{1}$$

Since mass can be expressed as the product of density (ρ) and volume (V), Equation (1) can be rewritten as the following Equation (2).

$$D = \frac{E_{dep}}{\rho V} \tag{2}$$

For a slab-shaped detector with a fixed cross-sectional area A and thickness t, its volume is given by V = A t, so dose on the silicon detector can be written as equation (3).

$$D(t) = \frac{E_{dep}(t)}{\rho\, A\, t} \tag{3}$$

Equation (3) shows that changes in silicon thickness (t) affect the deposited energy ($E_{dep}(t)$) and the volume (V) mass that receives the deposition. Therefore, the effect of thickness on TID was analyzed numerically using Monte Carlo simulations.

The T-Deposit calculation in PHITS provides the dose per source particle for each simulated thickness variation. The simulation results are expressed in Gy/source, representing the absorbed dose per primary particle (D_{sim}). The simulated dose values can be multiplied by the number of source particles (N) to obtain the total TID value (Equation (4)).

$$TID_{total} = D_{sim} \times N \tag{4}$$

III. RESULTS AND DISCUSSION

In this study, simulations were performed using two proton energy levels—25 MeV and 100 MeV—to represent primary particle conditions with different penetration capabilities and potentials for secondary particle formation. Variations in silicon detector thickness were grouped into two main categories—thin and bulk—so that differences in response between very thin sensitive volumes and larger active volumes could be observed more clearly. The simulated outputs analyzed include proton tracks as a representation of primary particle transport within the simulation geometry, secondary particle tracks in the form of photons and neutrons produced after proton interaction with the target, and the dose received by the silicon detector for all thickness variations at each energy level. Analysis of proton tracks and secondary particles is used to provide a physical picture of the transport mechanisms and the formation of radiation fields within the system, while dose analysis is used to quantitatively evaluate the effects of proton energy and detector thickness on the silicon dosimetry response. This 2D visualization of primary and secondary particle trajectories aims to provide a qualitative understanding of the interaction mechanisms underlying dose calculations, whereas quantitative analysis focuses on the total ionizing dose (TID) as an integrated measure of energy deposition. The statistical uncertainty of all simulations obtained in this study is less than 2%.

1) *Distribution of protons and secondary particles as a function of energy and detector thickness:* Figure 2 shows the two-dimensional (2D) distribution patterns of proton scattering in the x–z plane for four simulation conditions with two proton energy variations—25 MeV and 100 MeV—and two detector thickness variations—0.001 cm and 0.05 cm. Figure 2(a) represents 25 MeV energy with a thickness of 0.001 cm, (b) 25 MeV energy with a thickness of 0.05 cm, (c) 100 MeV energy with a thickness of 0.001 cm, and (d) 100 MeV energy with a

thickness of 0.05 cm. The color scale on the right side of each panel indicates flux magnitude, with red indicating higher intensity. These 2D maps show how protons move from the left side (particle source) toward the Al alloy target region and then continue their path toward the detector for various combinations of energy and thickness.

This figure shows that the most distinct difference is observed in the change in proton energy, while differences due to changes in detector thickness are not observed. At 25 MeV (Figures 2(a) and (b)), the proton spread after passing through the target region appears very limited and does not show significant penetration to the right, so the dominant flux distribution remains concentrated around the entry path and the region near the target. Protons are well absorbed in the Al alloy material. Conversely, at 100 MeV (Figures 2(c) and (d)), the protons appear to penetrate further in the positive z-axis direction with a longer spread pattern and a flux intensity that remains high along the main axis, indicating greater penetration at higher energies. This proton penetrated deeply enough to pass through the Si detector material. Meanwhile, when comparing thicknesses of 0.001 cm and 0.05 cm at the same energy, no significant difference is visible in this 2D map for both energy variations, which show nearly identical distribution shapes. Variations in detector thickness have not yet produced clear changes in the proton distribution pattern, whereas the increase in energy from 25 MeV to 100 MeV yields noticeable changes in the path length and the dominance of the proton flux within the simulation geometry.

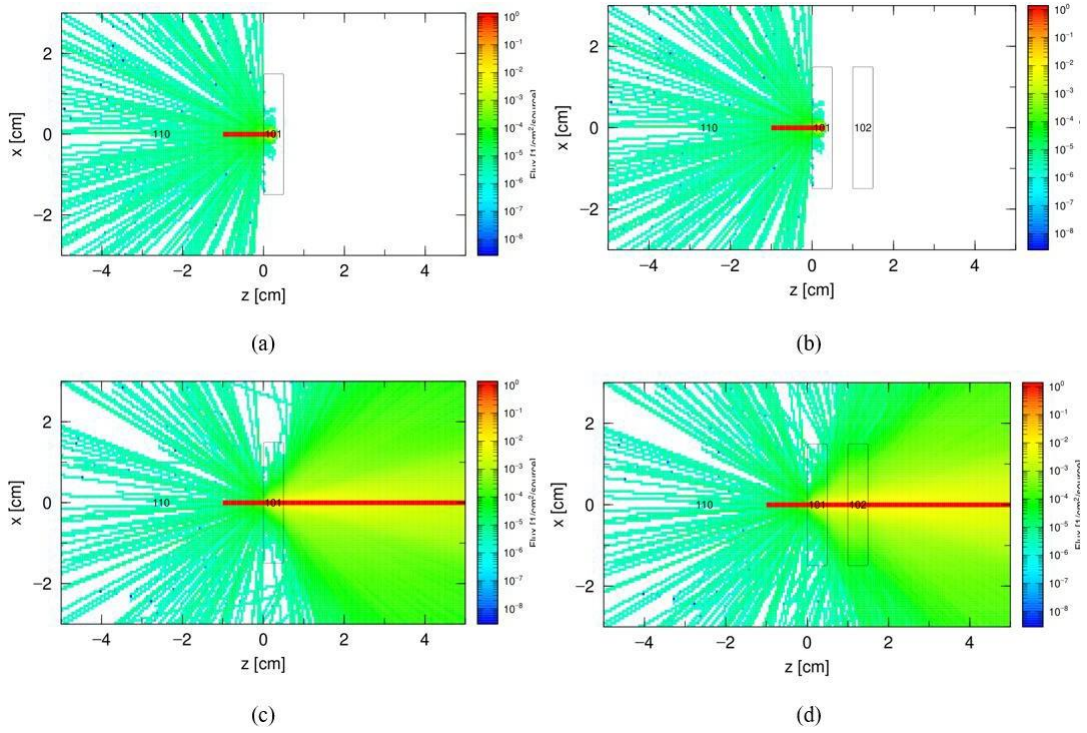

Fig. 2. 2D distribution of protons as a function of energy and thickness: (a) Energy: 25 MeV; thickness: 0.001 cm, (b) Energy: 25 MeV; thickness: 0.05 cm, (c) Energy: 100 MeV; thickness: 0.001 cm, and (d) Energy: 100 MeV; thickness: 0.05 cm

Protons interact with the Al alloy material, producing secondary particles in the form of photons and neutrons. The 2D maps of the secondary particle distribution for variations in energy and detector thickness are shown in Figures 3 and 4. These visualizations demonstrate how changes in proton energy affect the formation and distribution of secondary particles within the simulation geometry. In addition, these distribution maps also provide insight into whether variations in detector thickness result in changes in the distribution patterns of secondary particles that can be observed visually.

In this simulation, photons are generated when 25 MeV and 100 MeV protons interact with the aluminum alloy material in the target. The protons lose energy as they pass through the material via ionization and atomic excitation, which produces secondary electrons. These secondary electrons can emit photons through the process of bremsstrahlung as they are slowed down by the atomic nuclei within the material. Additionally, the interaction of protons with target atoms can also create excited states in the atoms or nuclei, which then release energy in the form of photons as they return to a more stable state [16-18]. The photons shown in the figure are an indirect result of the interaction of protons with the target material, and their presence reflects the transfer of energy from the

primary protons to the secondary radiation field. The differences in proton energy (25 MeV and 100 MeV) and detector thickness (0.001 cm and 0.05 cm) are not visually apparent in this 2D distribution map, as the color patterns and photon flux distributions in the four images appear nearly identical.

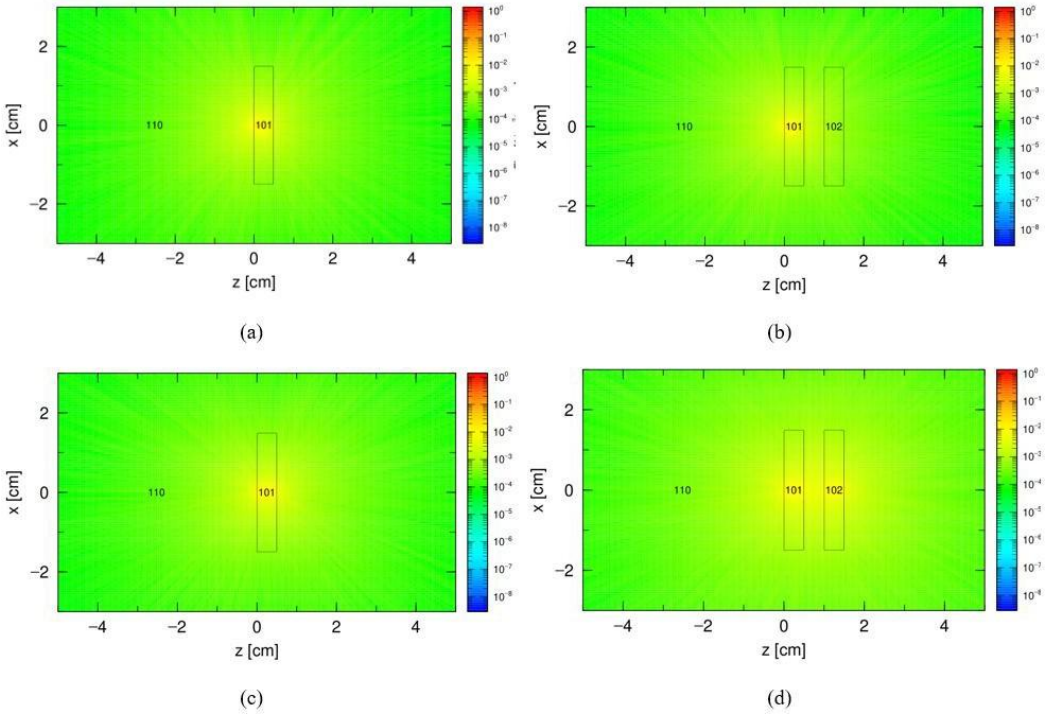

Fig. 3. 2D distribution of photons as a function of energy and thickness: (a) Energy: 25 MeV; thickness: 0.001 cm, (b) Energy: 25 MeV; thickness: 0.05 cm, (c) Energy: 100 MeV; thickness: 0.001 cm, and (d) Energy: 100 MeV; thickness: 0.05 cm

Another secondary particle is the neutron, which is also produced by the interaction of the Al alloy target material with protons. The neutron distribution pattern remains unchanged across different thicknesses. However, changes in proton energy result in different patterns (Figure 4). The figure shows that more neutrons are produced at higher energies because the probability of interaction is greater when the proton energy is increased.

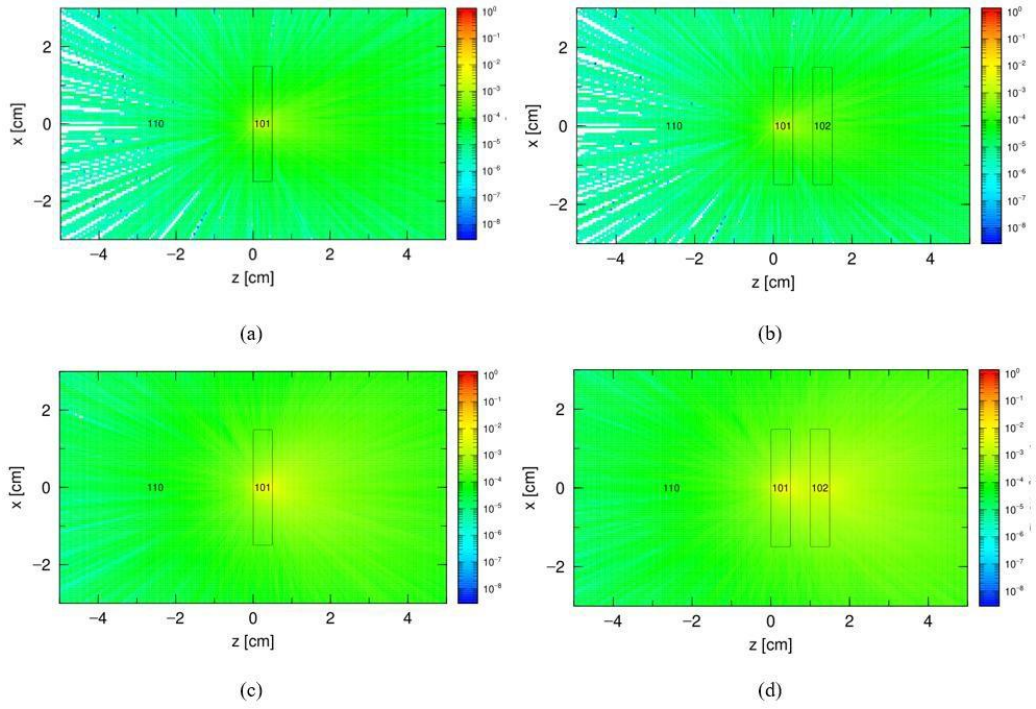

Fig. 4. 2D distribution of neutrons as a function of energy and thickness: (a) Energy: 25 MeV; thickness: 0.001 cm, (b) Energy: 25 MeV; thickness: 0.05 cm, (c) Energy: 100 MeV; thickness: 0.001 cm, and (d) Energy: 100 MeV; thickness: 0.05 cm

2) TID calculation: In addition to the distribution of protons and secondary particles, which represent the quantity of radiation, the Total Ionizing Dose (TID) parameter is also analyzed to evaluate the quality of the energy deposition received by the silicon detector as a result of exposure to protons and the resulting secondary particles. TID is an important parameter because it not only indicates the presence of radiation around the detector but also describes how much ionizing energy is actually absorbed by the sensitive material. In this context, the silicon detector was chosen because it is a semiconductor material highly relevant for radiation sensor applications, where its dosimetric response is influenced by direct interactions with primary protons as well as indirect interactions via secondary photons and neutrons. Therefore, TID analysis provides more representative information regarding the potential impact of radiation on the detector material compared to flux analysis alone. The TID is calculated using Equation (4) in units of Gy.

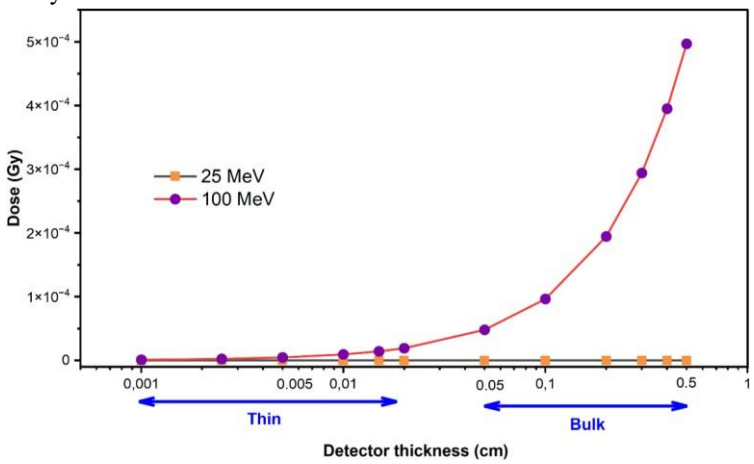

Fig. 5. Variation of TID with silicon detector thickness at proton energies of 25 MeV and 100 MeV

The relationship between variations in silicon detector thickness and TID values at proton energies of 25 MeV and 100 MeV is shown in Figure 5. In general, both energy levels exhibit the same trend: TID values increase with increasing detector thickness in both the thin and bulk groups. This increase indicates that the greater the thickness of the silicon's sensitive volume, the greater the energy that can be deposited within the detector. Increasing the thickness extends the effective path length of particle interactions within the material, thereby increasing the accumulation of energy deposition recorded as absorbed dose. Although both energy levels show a similar linear trend, the curve at 25 MeV appears flatter than that at 100 MeV. In the thin group, the dose remains relatively small due to the limited detector thickness and the increase in dose remains consistent with the increase in thickness. Meanwhile, in the bulk group, the dose values are significantly higher because the thicker active volume allows for greater energy deposition. Figure 4 confirms that detector thickness has a direct effect on TID and this effect becomes stronger at higher proton energies. Detector thickness has a direct effect on TID because an increase in thickness increases the effective interaction path length and the volume of energy deposition within the silicon. This effect becomes more pronounced at higher proton energies because higher-energy protons have greater penetrating power and are capable of sustaining the energy deposition process throughout the detector's thickness, accompanied by an additional contribution from secondary particles formed at the target [12], [19].

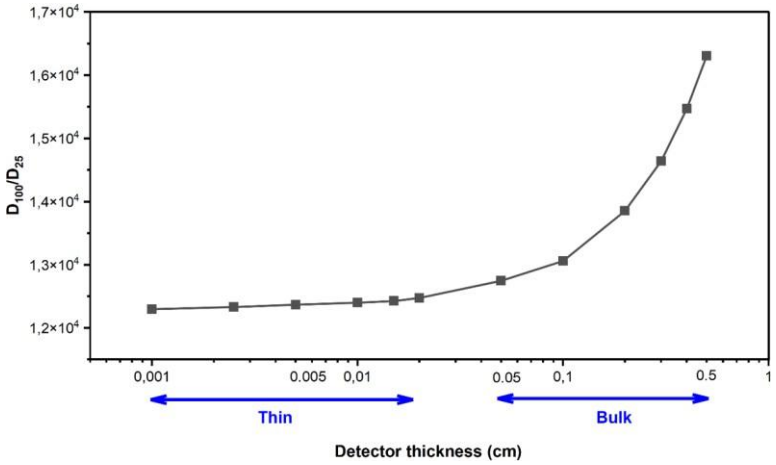

Fig. 6. Relative TID of silicon detectors at $D_{100}(t)/D_{25}(t)$ for each detector thickness

The difference in dosimetric response between the two energies is illustrated in Figure 6, which shows the ratio of $D_{100}(t)/D_{25}(t)$ for each detector thickness. This figure normalizes the effect of thickness and directly shows the magnitude of the dose increase at 100 MeV compared to 25 MeV at the same thickness. The ratio tends to increase with greater thickness, indicating that the effect of proton energy becomes increasingly significant in thicker sensitive volumes. The TID results in Figures 5 and 6 are consistent with the distributions of protons and secondary particles discussed earlier. At an energy of 100 MeV, protons have greater penetration and longer track lengths, thereby increasing the probability of energy deposition within the silicon. The increase in proton energy responsible for this rise in the TID value is consistent with findings from other study [7]. On the other hand, proton interactions with the target also produce secondary particles such as photons and neutrons, which contribute to energy deposition in the detector. Therefore, the increase in TID at higher energies is not only related to the dominance of primary protons but also to the secondary radiation field formed around the detector. This relationship indicates that the particle distribution within the simulation geometry plays a direct role in shaping the silicon dosimetry response so that flux and TID analyses complement each other in explaining the radiation characteristics of the simulation system with the detector thickness 0.001 – 0.5 cm.

IV. CONCLUSION

Proton energy and silicon detector thickness have different effects on the particle transport characteristics and dosimetric response of the system under study. The proton distribution shows a clear difference between 25 MeV and 100 MeV energies, where 100 MeV protons have a longer transport range and more dominant penetration within the simulation geometry, whereas the effect of extreme thickness variations on the proton distribution pattern is not visually prominent. The distribution of secondary particles, namely photons and neutrons, across all energy and thickness variations also exhibits relatively similar patterns, so that the differences cannot be clearly distinguished from the obtained 2D maps. Furthermore, the simulation results indicate that the TID value increases linearly with increasing silicon detector thickness for both 25 MeV and 100 MeV proton energies, with the TID value at 100 MeV consistently higher than that at 25 MeV across all thickness variations. These findings confirm that within the range of parameters examined, detector thickness plays a direct role in determining the magnitude of TID, while an increase in proton energy systematically enhances the dosimetric response of the silicon detector.

REFERENCES

[1] A. Karmakar, J. Wang, J. Prinzie, V. De Smedt, and P. Leroux, “A Review of Semiconductor Based Ionising Radiation Sensors Used in Harsh Radiation Environments and Their Applications,” Radiation, vol. 1, no. 3, pp. 194–217, Sep. 2021, doi: 10.3390/radiation1030018.

[2] I. Jun et al., “A review on radiation environment pathways to impacts: Radiation effects, relevant empirical environment models, and future needs,” Adv. Space Res., Apr. 2024, doi: 10.1016/j.asr.2024.03.079.

[3] J. Cardenas Chavez, D. Hiemstra, A. Noguera Cundar, B. Johnson, D. Baik, and L. Chen, “Total Ionizing Dose and Single-Event Effect Response of the AD524CDZ Instrumentation Amplifier,” Energies, vol. 17, no. 18, p. 4725, Jan. 2024, doi: 10.3390/en17184725.

[4] J. Yang, G. Ma, X. Li, C. Liu, D. Yang, and S. He, “Effects of multilayer and multimaterial structures on space proton radiation protection,” Nucl. Instrum. Methods Phys. Res. Sect. B Beam Interact. Mater. At., vol. 365, pp. 352–356, Dec. 2015, doi: 10.1016/j.nimb.2015.08.054.

[5] Z. Liu, B. Li, J. Quan, and J. Luo, “Total-Ionization-Dose Radiation Effects and Hardening Techniques of a Mixed-Signal Spike Neural Network in 180 nm SOI-Pavlov Process,” Electronics, vol. 11, no. 10, p. 1643, Jan. 2022, doi: 10.3390/electronics11101643.
[6] Z. Liu et al., “Impact of proton-induced total ionizing dose effects on electrical characteristics and safe operating area of trench field-stop IGBT devices,” Microelectron. Reliab., vol. 154, p. 115326, Mar. 2024, doi: 10.1016/j.microrel.2024.115326.
[7] G. D. H et al., “High-energy electron measurements with thin Si detectors,” Measurement, vol. 228, p. 114392, Mar. 2024, doi: 10.1016/j.measurement.2024.114392.
[8] J. M. Rafí et al., “Ultrathin four-quadrant silicon photodiodes for beam position and monitor applications: Characterization and radiation effects,” Solid-State Electron., vol. 209, p. 108756, Nov. 2023, doi: 10.1016/j.sse.2023.108756.
[9] H. Park et al., “Development of accurate dose evaluation technique of X-ray inspection for quality assurance of semiconductor with Monte Carlo simulation,” Appl. Radiat. Isot., vol. 154, p. 108851, Dec. 2019, doi: 10.1016/j.apradiso.2019.108851.
[10] M. Liu et al., “Analysis of Difference in Areal Density Aluminum Equivalent Method in Ionizing Total Dose Shielding Analysis of Semiconductor Devices,” Electronics, vol. 12, no. 19, p. 4181, Jan. 2023, doi: 10.3390/electronics12194181.
[11] K. Sedlačková, B. Zaťko, A. Šagátová, and V. Nečas, “Monte Carlo simulations of the particle transport in semiconductor detectors of fast neutrons,” Nucl. Instrum. Methods Phys. Res. Sect. Accel. Spectrometers Detect. Assoc. Equip., vol. 709, pp. 63–67, May 2013, doi: 10.1016/j.nima.2013.01.011.
[12] A. Fetzer, M. Anger, P. Oleynik, and J. Praks, “Total ionising dose multilayer shielding optimisation for nanosatellites on geostationary transfer orbit,” Adv. Space Res., vol. 73, no. 1, pp. 831–845, Jan. 2024, doi: 10.1016/j.asr.2023.10.028.
[13] T. Sato et al., “Features of Particle and Heavy Ion Transport code System (PHITS) version 3.02,” J. Nucl. Sci. Technol., vol. 55, no. 6, pp. 684–690, Jun. 2018, doi: 10.1080/00223131.2017.1419890.
[14] P. Papadimitroulas, “Dosimetry applications in GATE Monte Carlo toolkit,” Phys. Med., vol. 41, pp. 136–140, Sep. 2017, doi: 10.1016/j.ejmp.2017.02.005.
[15] R. Danieli et al., “Personalized Dosimetry in Targeted Radiation Therapy: A Look to Methods, Tools and Critical Aspects,” J. Pers. Med., vol. 12, no. 2, p. 205, Feb. 2022, doi: 10.3390/jpm12020205.
[16] S. H. Park and J. O. Kang, “Basics of particle therapy I: physics,” Radiat. Oncol. J., vol. 29, no. 3, pp. 135–146, Sep. 2011, doi: 10.3857/roj.2011.29.3.135.
[17] F. Folkmann, C. Gaarde, T. Huus, and K. Kemp, “Proton induced X-ray emission as a tool for trace element analysis,” Nucl. Instrum. Methods, vol. 116, no. 3, pp. 487–499, Apr. 1974, doi: 10.1016/0029-554X(74)90831-3.
[18] M. Pinto, “Prompt-gamma imaging in particle therapy,” Eur. Phys. J. Plus, vol. 139, no. 10, p. 884, Oct. 2024, doi: 10.1140/epjp/s13360-024-05664-4.
[19] A. Pehlivanlı and M. H. Bölükdemir, “Investigation of the effects of biomaterials on proton Bragg peak and secondary neutron production by the Monte Carlo method in the slab head phantom,” Appl. Radiat. Isot., vol. 180, p. 110060, Feb. 2022, doi: 10.1016/j.apradiso.2021.110060.